



# THE UNIVERSITY *of* EDINBURGH

## Edinburgh Research Explorer

### Virtual Analog Model of the Lockhart Wave Folder

**Citation for published version:**

Esqueda, F, Poyntinen, H, Parker, J & Bilbao, S 2017, Virtual Analog Model of the Lockhart Wave Folder. in Proceedings of the 14th Sound and Music Computing Conference. Aalto University.

**Link:**

[Link to publication record in Edinburgh Research Explorer](#)

**Document Version:**

Publisher's PDF, also known as Version of record

**Published In:**

Proceedings of the 14th Sound and Music Computing Conference

**General rights**

Copyright for the publications made accessible via the Edinburgh Research Explorer is retained by the author(s) and / or other copyright owners and it is a condition of accessing these publications that users recognise and abide by the legal requirements associated with these rights.

**Take down policy**

The University of Edinburgh has made every reasonable effort to ensure that Edinburgh Research Explorer content complies with UK legislation. If you believe that the public display of this file breaches copyright please contact [openaccess@ed.ac.uk](mailto:openaccess@ed.ac.uk) providing details, and we will remove access to the work immediately and investigate your claim.



## Virtual Analog Model of the Lockhart Wavefolder

**Fabián Esqueda, Henri Pöntynen**

Dept. of Signal Processing and Acoustics  
Aalto University  
Espoo, Finland

fabian.esqueda@aalto.fi  
henri.pontynen@aalto.fi

**Julian D. Parker**

Native Instruments GmbH  
Berlin, Germany

julian.parker@native-instruments.de

**Stefan Bilbao**

Acoustics and Audio Group  
University of Edinburgh  
Edinburgh, UK

s.bilbao@ed.ac.uk

### ABSTRACT

This work presents a novel virtual analog model of the Lockhart wavefolder. Wavefolding modules are among the fundamental elements of 'West Coast' style analog synthesis. These circuits produce harmonically-rich waveforms when driven by simple periodic signals such as sinewaves. Since wavefolding introduces high levels of harmonic distortion, we pay special attention to suppressing aliasing without resorting to high oversampling factors. Results obtained are validated against SPICE simulations of the original circuit. The proposed model preserves the nonlinear behavior of the circuit without perceivable aliasing. Finally, we propose a practical implementation of the wavefolder using multiple cascaded units.

### 1. INTRODUCTION

In 1965, Bob Moog (1934–2005) presented his seminal work on the design of a voltage-controlled filter (VCF) at the 17<sup>th</sup> Annual AES Meeting [1]. Moog's design became a key element of the celebrated Moog sound and of electronic music in general. His work paved the way for the development of a synthesis style known as "East Coast" synthesis, named after Moog's New York origins. Two years prior, in 1963, the San Francisco Tape Music Center, along with composers Morton Subotnick and Ramon Sender, commissioned a voltage-controlled instrument from the Berkeley-based Don Buchla (1937–2016). This led to the development of Buchla's first synthesizer, the Buchla 100, and the birth of "West Coast" synthesis [2].

Although contemporaries, the synthesis paradigms of Moog and Buchla had very little in common. In East Coast synthesis, sounds are sculpted by filtering harmonically-rich waveforms, such as sawtooth or square waves, with a resonant filter. This approach is known in the literature as subtractive synthesis. In contrast, West Coast synthesis eschews traditional filters and instead manipulates harmonic content, or timbre, at oscillator level using a variety of techniques such as waveshaping and frequency modulation. The resulting waveforms are then processed with a

lowpass gate (LPG), a filter/amplifier circuit that uses photoresistive opto-isolators, or vactrols, in its control path [3]. To set them apart from their East Coast counterparts, West Coast oscillators are called "complex oscillators".

One of Buchla's early waveform generators featured a wavefolding circuit designed to control timbre. Wavefolding is a type of nonlinear waveshaping where portions of a waveform are inverted or "folded back" on itself. When driven by a signal with low harmonic content, e.g. a sine or triangular oscillator, wavefolders can generate harmonically-rich waveforms with distinctive tonal qualities. This work presents a novel virtual analog (VA) model of the Lockhart wavefolder, a West Coast-style circuit proposed by Ken Stone as part of his CGS synthesizer and available as a DIY project on his personal website [4].

Recent years have seen an increase in the number of manufacturers embracing West Coast synthesis and releasing their own takes on classic Buchla and Serge (another famed West Coast designer of the 1970s) modules. Modern synthesizer makers, such as Make Noise, Intellijel and Doepfer, all feature complex oscillators and LPGs in their product lines. This growing interest in modular synthesizers, which are generally exclusively expensive, serves as the principal motivation behind the development of VA models of these circuits. VA synthesizers are generally affordable and are exempt from the inherent limitations of analog circuits, e.g. faults caused by aging components.

An essential requirement in VA modeling is to preserve the "analog warmth" of the original circuit [5,6]. This perceptual attribute is associated with the nonlinear behavior inherent to semiconductor devices and vacuum tubes, and can be modeled via large-signal circuit analysis. This approach has been researched extensively in the context of VCFs [7–11] and effects processing [12–19]. The use of nonlinear waveshaping in digital sound synthesis is also well documented [20–23].

A particular challenge in VA models of nonlinear devices is aliasing suppression. High oversampling factors are usually necessary to prevent harmonics introduced by nonlinear processing from reflecting to the baseband as aliases. Aliasing reduction has been widely studied in the context of waveform synthesis [24–30]. Moreover, recent work has extended the use of a subset of these techniques to special processing cases such as signal rectification and hard clipping [31,32]. The proposed Lockhart VA model incorporates the antiderivative antialiasing method proposed by

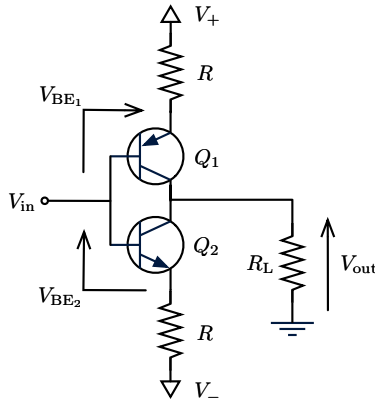


Figure 1. Schematic of the Lockhart wavfolder circuit.

Parker et al. [33, 34].

This paper is organized as follows. Sections 2 and 3 focus on the analysis of the Lockhart circuit and derivation of an explicit model. Section 4 deals with the digital implementation of the model. Section 5 discusses synthesis topologies based around the proposed wavfolder. Finally, Section 6 provides concluding remarks and thoughts for further work.

## 2. CIRCUIT ANALYSIS

Figure 1 shows a simplified schematic of the Lockhart wavfolder adapted from Ken Stone's design [4]. This circuit was originally designed to function as a frequency tripler by R. Lockhart Jr. [4, 35], but was later repurposed to perform wavfolding in analog synthesizers. The core of the circuit consists of an NPN and a PNP bipolar junction transistor tied at their base and collector terminals. In order to carry out the large-signal analysis of the circuit, we replace  $Q_1$  and  $Q_2$  with their corresponding Ebers-Moll injection models [10] as shown in Figure 2. Nested subscripts are used to distinguish between the currents and voltages in  $Q_1$  from those in  $Q_2$ . For instance,  $I_{CD_1}$  is the current through the collector diode in  $Q_1$ .

We begin our circuit analysis by assuming that the supply voltages  $V_{\pm}$  will always be significantly larger than the voltage at the input, i.e.  $V_- < V_{in} < V_+$ . This assumption is valid for standard synthesizer voltage levels ( $V_{\pm} = \pm 15V$ ,  $V_{in} \in [-5, 5]V$ ), and implies that the base-emitter junctions of  $Q_1$  and  $Q_2$  will be forward-biased with approximately constant voltage drops for all expected input voltages. Applying Kirchhoff's voltage law around both input-emitter loops (cf. Fig. 1) results in

$$V_{in} = V_+ - RI_{E_1} - V_{BE_1}, \quad (1)$$

$$V_{in} = V_{BE_2} + RI_{E_2} + V_-, \quad (2)$$

where  $I_{E_1}$  and  $I_{E_2}$  are the emitter currents, and  $V_{BE_1}$  and  $V_{BE_2}$  are the voltage drops across the base-emitter junctions of  $Q_1$  and  $Q_2$ , respectively. Solving (1) and (2) for

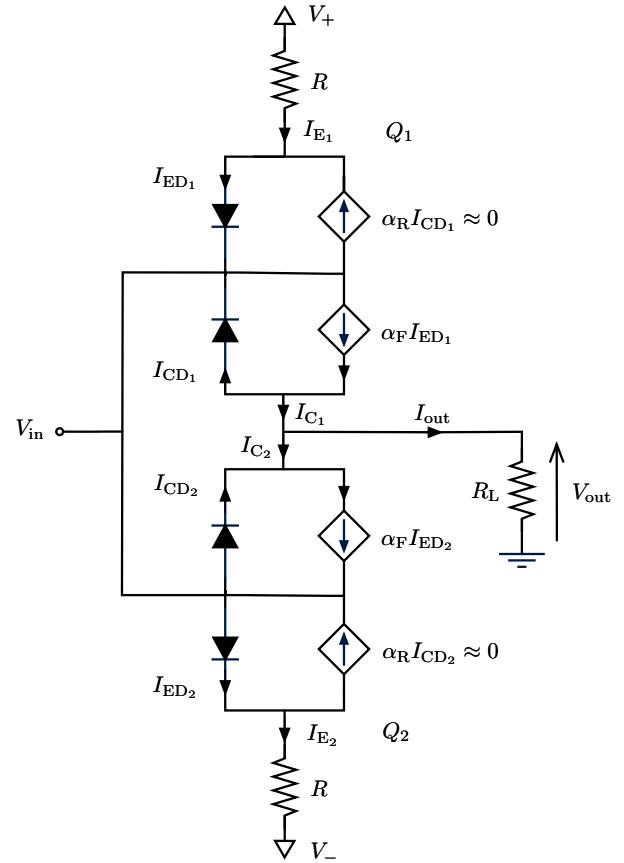


Figure 2. Ebers-Moll equivalent model of the Lockhart wavfolder circuit.

the emitter currents then yields:

$$I_{E_1} = \frac{V_+ - V_{BE_1} - V_{in}}{R}, \quad (3)$$

$$I_{E_2} = \frac{V_{in} - V_{BE_2} - V_-}{R}. \quad (4)$$

Next, we apply Kirchhoff's current law at the collector nodes:

$$I_{out} = I_{C_1} - I_{C_2}, \quad (5)$$

$$I_{C_1} = \alpha_F I_{ED_1} - I_{CD_1}, \quad (6)$$

$$I_{C_2} = \alpha_F I_{ED_2} - I_{CD_2}. \quad (7)$$

Assuming that the contribution of reverse currents  $\alpha_R I_{CD_1}$  and  $\alpha_R I_{CD_2}$  to the total emitter currents  $I_{ED_1}$  and  $I_{ED_2}$  is negligible, we can establish that

$$I_{ED_1} \approx I_{E_1} \quad \text{and} \quad I_{ED_2} \approx I_{E_2}.$$

Substituting these values in (6) and (7), and setting the value  $\alpha_F = 1$  gives a new expression for the output current:

$$I_{out} = I_{E_1} - I_{E_2} - I_{CD_1} + I_{CD_2}. \quad (8)$$

Combining (3) and (4) we can derive an expression for the difference between emitter currents. Since the voltage drops  $V_{BE_1}$  &  $V_{BE_2}$  across the base-emitter junctions are

approximately equal (i.e.  $V_{BE_1} \approx V_{BE_2}$ ) for the expected range of  $V_{in}$ , their contribution to the difference of emitter currents vanishes. Therefore,

$$I_{E_1} - I_{E_2} = -\frac{2V_{in}}{R}. \quad (9)$$

Substituting (9) into (8) yields an expression for the total output current  $I_{out}$  in terms of the input voltage and the currents through the collector diodes:

$$I_{out} = -\frac{2V_{in}}{R} - I_{CD_1} + I_{CD_2}. \quad (10)$$

Now, the I-V relation of a diode can be modeled using Shockley's ideal diode equation, defined as

$$I_D = I_S \left( e^{\frac{V_D}{\eta V_T}} - 1 \right), \quad (11)$$

where  $I_D$  is the diode current,  $I_S$  is the reverse bias saturation current,  $V_T$  is the thermal voltage and  $\eta$  is the ideality factor of the diode. Applying Shockley's diode equation to the collector diodes using ideality factor  $\eta = 1$ , and substituting into (10) gives us

$$I_{out} = -\frac{2V_{in}}{R} - I_S \left( e^{\frac{V_{CD_1}}{V_T}} - e^{\frac{V_{CD_2}}{V_T}} \right). \quad (12)$$

Next, we use Kirchhoff's voltage law to define expressions for  $V_{CD_1}$  and  $V_{CD_2}$  in terms of  $V_{in}$  and  $V_{out}$

$$V_{CD_1} = V_{out} - V_{in}, \quad (13)$$

$$V_{CD_2} = V_{in} - V_{out}, \quad (14)$$

and replace these values in (12). This gives us

$$I_{out} = -\frac{2V_{in}}{R} - I_S \left( e^{\frac{V_{out}-V_{in}}{V_T}} - e^{\frac{V_{in}-V_{out}}{V_T}} \right). \quad (15)$$

As a final step, we multiply both sides of (15) by the load resistance  $R_L$  and remove the exponential functions to produce an expression for the output voltage of the Lockhart wavfolder:

$$V_{out} = -\frac{2R_L V_{in}}{R} - 2R_L I_S \sinh \left( \frac{V_{out} - V_{in}}{V_T} \right). \quad (16)$$

### 3. EXPLICIT FORMULATION

Equation (16) describes a nonlinear implicit relationship between the input and output voltages. Its solution can be approximated using numerical methods such as Halley's method or Newton-Raphson. These methods have previously been used in the context of VA modeling, e.g. in [10, 13, 16].

In this work, we propose an explicit formulation for the output voltage of the Lockhart wavfolder derived using the Lambert-W function. The Lambert-W function<sup>1</sup>  $W(x)$  is defined as the inverse function of  $x = ye^y$ , i.e.  $y = W(x)$ . Recent research has demonstrated its suitability for VA applications. Parker and D'Angelo used it

<sup>1</sup> Strictly speaking,  $W(x)$  is multivalued. This work only utilizes the upper branch, often known as  $W_0(x)$  in the literature.

to model the control circuit of the Buchla LPG [3]. Several authors have used it to solve the implicit voltage relationships of diode pairs [3, 36, 37]. As described in [36],  $W(x)$  can be used to solve problems of the form

$$(A + Bx)e^{Cx} = D, \quad (17)$$

which have the solution

$$x = \frac{1}{C} W \left( \frac{CD}{B} e^{AC/B} \right) - \frac{A}{B}. \quad (18)$$

Since the collector diodes in the model are antiparallel, only one of them can conduct at a time [38]. Going back to (10), when  $V_{in} \geq 0$  virtually no current flows through the collector diode of  $Q_1$  (i.e.  $I_{CD_1} \approx 0$ ). The same can be said for  $I_{CD_2}$  when  $V_{in} < 0$ . By combining these new assumptions with (12)–(14), we can derive a piecewise expression for the Lockhart wavfolder:

$$V_{out} = -\frac{2R_L}{R} V_{in} + \lambda R_L I_S \exp \left( \frac{\lambda(V_{in} - V_{out})}{V_T} \right), \quad (19)$$

where  $\lambda = \text{sgn}(V_{in})$  and  $\text{sgn}()$  is the *signum* function.

This expression is still implicit; however, it can be rearranged in the form described by (17), which gives us:

$$\left( \frac{2R_L}{R} V_{in} + V_{out} \right) \exp \left( \frac{\lambda V_{out}}{V_T} \right) = \lambda R_L I_S \exp \left( \frac{\lambda V_{in}}{V_T} \right) \quad (20)$$

Solving for  $V_{out}$  as defined in (18) yields an explicit model for the Lockhart wavfolder:

$$V_{out} = \lambda V_T W(\Delta \exp(\lambda \beta V_{in})) - \alpha V_{in}, \quad (21)$$

where

$$\alpha = \frac{2R_L}{R}, \quad \beta = \frac{R + 2R_L}{V_T R} \quad \text{and} \quad \Delta = \frac{R_L I_S}{V_T}. \quad (22)$$

An important detail to point out is that the output of the Lockhart wavfolder is out of phase with the input signal by 180°. This can be compensated with a simple inverting stage.

### 4. DIGITAL IMPLEMENTATION

The voltages and currents inside an electronic circuit are time-dependent. Therefore, the Lockhart wavfolder can be described as a nonlinear memoryless system of the form

$$V_{out}(t) = f(V_{in}(t)), \quad (23)$$

where  $f$  is the nonlinear function (21) and  $t$  is time. Equation (24) can then be discretized directly as

$$V_{out}[n] = f(V_{in}[n]), \quad (24)$$

where  $n$  is the discrete-time sample index.

#### 4.1 Aliasing Considerations

The highly nonlinear behavior of (21) poses a challenge for its accurate discrete-time implementation. As an arbitrary input waveform is folded, new harmonics will be introduced. Those harmonics whose frequency exceeds half the sampling rate, or the Nyquist limit, will be reflected into the baseband and will cause unpleasant artifacts. Oversampling by high factors is commonly employed to mitigate this problem but this approach increases the computational requirements of the system by introducing redundant operations.

In this work, we propose using the first-order antiderivative method presented in [33] and [34]. This method is derived from the analytical convolution of a continuous-time representation of the processed signal with a first-order lowpass kernel. The antialiased form for the Lockhart wavefolder is given by

$$V_{\text{out}}[n] = \frac{F(V_{\text{in}}[n]) - F(V_{\text{in}}[n-1])}{V_{\text{in}}[n] - V_{\text{in}}[n-1]}, \quad (25)$$

where  $F()$  is the antiderivative of  $f()$ , the wavefolder function (21). This antiderivative is defined as

$$F(V_{\text{in}}) = \frac{V_{\text{T}}}{2\beta} (1 + W(\Delta \exp(\lambda\beta V_{\text{in}})))^2 - \frac{\alpha}{2} V_{\text{in}}^2. \quad (26)$$

Since the antiderivative of  $W$  is defined in terms of  $W$  itself, this form provides a cheap alternative to oversampling. This means the value  $W$ , which constitutes the most computationally expensive part of both (21) and (26), only has to be computed once for each output sample.

Now, when  $V_{\text{in}}[n] \approx V_{\text{in}}[n-1]$  (25) becomes ill-conditioned. This should be avoided by defining the special case

$$V_{\text{out}}[n] = f\left(\frac{V_{\text{in}}[n] + V_{\text{in}}[n-1]}{2}\right), \quad (27)$$

when  $|V_{\text{in}}[n] - V_{\text{in}}[n-1]|$  is smaller than a predetermined threshold, e.g.  $10^{-6}$ . This special case simply bypasses the antialiased form while compensating for the half-sample delay introduced by the method.

#### 4.2 Computing the Lambert-W Function

Several options exist to compute the value of  $W(x)$ . In fact, scripting languages such as MATLAB usually contain their own native implementations of the function. Paiva et al. [38] proposed the use of a simplified iterative method which relied on a table-read for its initial guess. In the interest of avoiding lookup tables, we propose approximating the value of the Lambert-W function directly using Halley's method, as suggested in [39]. To compute  $w_m$ , an approximation to  $W(x)$ , we iterate over

$$w_{m+1} = w_m - \frac{p_m}{p_m s_m - r_m}, \quad (28)$$

where

$$\begin{aligned} p_m &= w_m e^{w_m} - x, \\ r_m &= (w_m + 1)e^{w_m}, \\ s_m &= \frac{w_m + 2}{2(w_m + 1)}, \end{aligned}$$

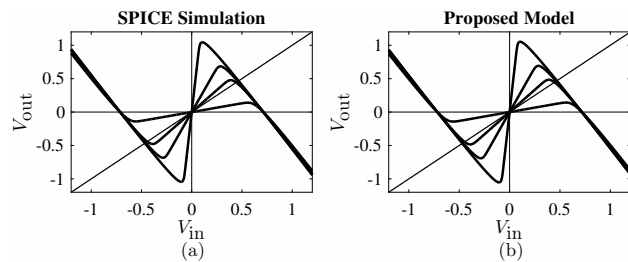


Figure 3. Input–output relationship of the Lockhart wavefolder circuit (inverted) measured using (a) SPICE and (b) the proposed digital model, for load resistor values  $R_L = 1\text{k}, 5\text{k}, 10\text{k}$  and  $50\text{k}\Omega$  (in order of increasing steepness).

and  $m = 0, 1, 2, \dots, M - 1$ .  $M$  is then the number of iterations required for  $p_m$  to approximate zero. The efficiency of the method will then depend on the choice of the initial guess  $w_0$ . An optimized MATLAB implementation of this method can be found in [40].

## 5. RESULTS

To validate the proposed model, the circuit was simulated using SPICE. Figure 3(a) shows the input–output relationship of the system measured with SPICE for values of  $V_{\text{in}}$  between  $-1.2$  and  $1.2$  V and different load resistance values. Figure 3(b) shows the input–output relation of the proposed model (21) simulated using MATLAB. The polarity of the transfer function was inverted to compensate for the introduced phase shift. An ad hoc scaling factor of 2 was used on both measurements to compensate for the energy loss at the fundamental frequency. The results produced by the proposed model fit those produced by SPICE closely. As the value of the load resistor  $R_L$  is raised, the steepness of the wavefolder function increases. This increase in steepness translates into more abrasive tones at the output.

Figures 4(a) and (b) show the output of the wavefolder model when driven by a 500-Hz sinewave with a peak amplitude of 1 V, and  $R_L = 10\text{k}$  and  $50\text{k}\Omega$ , respectively. Both curves are plotted on top of their equivalent SPICE simulations, showing a good match. The original input signal has been included to help illustrate the folding operation performed by the system.

Figure 5(b) shows the magnitude spectrum of a 1-V sinewave with fundamental frequency  $f_0 = 2145$  Hz processed by the trivial (i.e. non-antialiased) wavefolder model (21). A sample rate  $F_s = 88.2$  kHz (i.e. twice the standard 44.1 kHz audio rate), was used in this and the rest of the examples presented in this study. This plot shows the high levels of aliasing distortion introduced by the wavefolding process, even when oversampling by factor 2 is used. Figure 5(d) shows the magnitude spectrum of the same waveform processed using the antialiased form (25). As expected, the level of aliasing has been significantly reduced, with very few aliases left above the  $-80$  dB mark. As illustrated by the left-hand side of Fig. 5, the antialiased form preserves the time-domain behavior of the system.

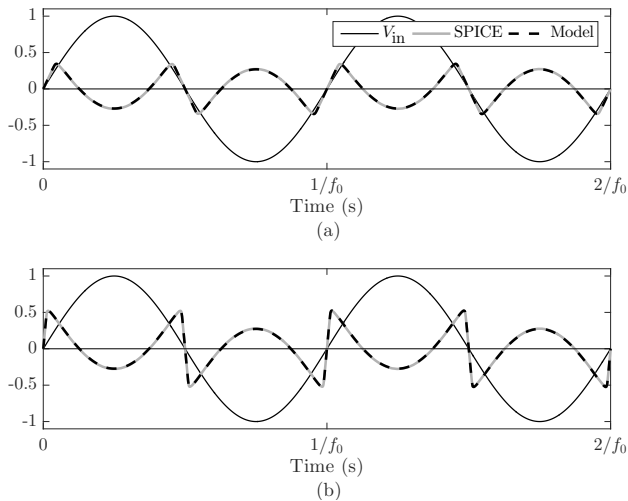


Figure 4. Time-domain view of the circuit’s SPICE simulation vs the proposed model for a 500-Hz sinusoidal input with values of  $R_L =$  (a)  $10\text{ k}\Omega$  and (b)  $50\text{ k}\Omega$ .

The proposed antialiased form is particularly effective at reducing aliased components at low frequencies, especially below the fundamental. This behavior is illustrated in Fig. 6 which shows the logarithmic magnitude spectrum of a 4186-Hz sinewave (MIDI note C8 and highest fundamental frequency of a piano) processed both trivially and with the antialiasing form. The signal depicted by Fig. 6(a) suffers from a false perceived fundamental frequency at roughly 300 Hz. For the case of the antialiased signal in Fig. 6(b) this issue has been ameliorated. This low-frequency behavior is advantageous in our case because at low frequencies the audibility of aliasing distortion is only limited by the hearing threshold [41].

The performance of the antialiased model form was further evaluated by computing the A-weighted noise-to-mask ratio (ANMR) for a range of folded sinusoidal inputs. The ANMR has been previously suggested as a perceptually-informed measure to evaluate the audibility of aliasing distortion [28, 41]. The algorithm computes the power ratio between harmonics and aliasing components, but takes into account the masking effects of the former. For instance, aliases clustered around harmonics will be rendered inaudible by the auditory masking effects of such harmonics. This phenomenon is particularly common at high frequencies. An A-weighting filter is applied to all signals prior to evaluation to account for the frequency-dependent sensitivity of hearing for low-level sounds [41]. Signals with an ANMR value below  $-10\text{ dB}$  are considered to be free from audible aliasing.

Figure 7 compares the measured ANMRs of a set of unit-amplitude sinewaves with fundamental frequencies between 1–5 kHz processed by the wavefolder model using the antialiasing form and different oversampling factors. The reference signals required to compute the ANMR values were generated using additive synthesis as detailed in [28]. All signals were downsampled back to audio rate (i.e. 44.1 kHz) prior to evaluation. This plot demonstrates that the performance of the proposed method, when com-

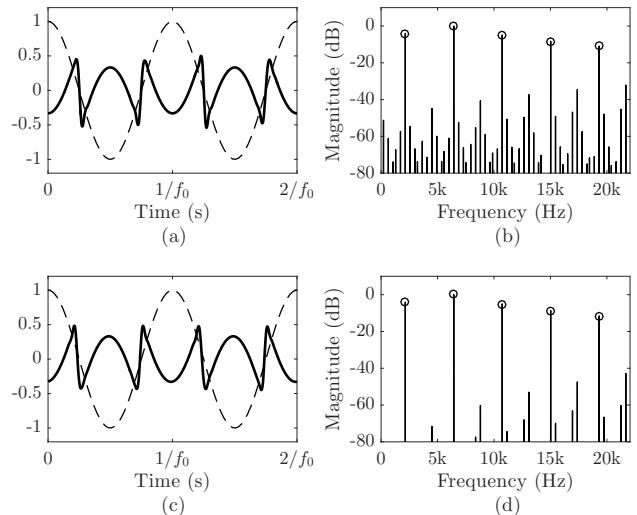


Figure 5. Waveform and magnitude spectrum of a 2145-Hz unit amplitude sinewave (a)–(b) processed trivially and (c)–(d) with the first-order antialiased form. Circles indicate non-aliased components. Parameter  $R_L = 50\text{ k}\Omega$ .

bined with two-times oversampling, is on par with oversampling by factor 8. For all fundamental frequencies below approx. 4.2 kHz the ANMR lies below the  $-10\text{ dB}$  line. In terms of computational costs, the antialiasing method is approx. four times cheaper than trivial oversampling by 8 when measured under similar circumstances.

## 6. PRACTICAL SYNTHESIS USAGE

In practical sound synthesis applications an individual wavefolder is rarely used as the timbral variety it can produce is quite limited. Most designs, for example the Intellijel  $\mu$ Fold, employ a number of wavefolding stages in series with intermediate gain elements used to space the folds. The number of stages varies between designs, and is in fact user variable in some cases. Typically somewhere between two and six folders are used.

Timbral control is then achieved using two parameters. The first is the gain at the input of the wavefolder. This parameter allows the overall brightness of the sound to be varied, and can be used to provide articulation to a sound similarly to a filter in subtractive synthesis or modulation index in FM synthesis. The second parameter is provided by adding a DC offset to the input of the wavefolder. This

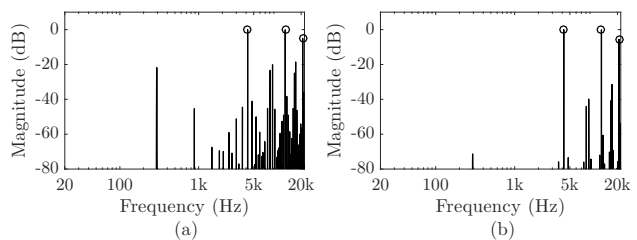


Figure 6. Log scale magnitude spectrum of a 4186-Hz sinewave (a) folded trivially and (b) with antialiasing. Parameter  $R_L = 50\text{ k}\Omega$ .

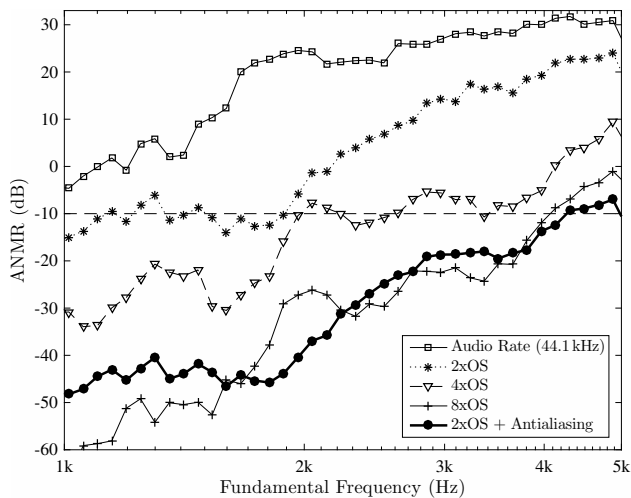


Figure 7. Measured ANMR of a range of sinusoidal waveforms processed using the Lockhart wavefolder model ( $R_L = 50 \text{ k}\Omega$ ) under five different scenarios: direct audio rate, oversampling by factors 2, 3 and 8, and oversampling by 2 combined with the antialiasing form. Values below the  $-10 \text{ dB}$  threshold indicate lack of perceivable aliasing.

breaks the symmetry of the folding and varies the relative amplitudes of the harmonics, without strongly effecting the overall brightness of the sound. This parameter can be modulated, e.g. with a low-frequency-oscillator (LFO), to provide an effect reminiscent of pulse-width modulation (PWM).

In order to build a well-behaved cascade of wavefolders, we need to make sure the individual folders satisfy two criteria. Firstly, the individual folders must provide approximately unity gain when  $V_{in} \approx 0$ , and approximately negative unit gain beyond the folding point, when  $|V_{in}| \gg 0$ . Secondly, each stage should start folding at the same point with respect to its individual input. We can achieve this with the model described above by appropriate setting of  $R_L$  and the addition of static pre- and post-gain stages.

An appropriate  $R_L$  can be determined empirically. The pre- and post- gain can be determined by measuring the value of  $V_{out}$  at exactly the folding point. The pre-gain is taken to be approximately this value, and the post-gain is taken to be its inverse. In this case,  $R_L = 7.5 \text{ k}\Omega$  was chosen, which leads to pre- and post-gains of approx.  $1/4$  and  $4$ , respectively.

The proposed structure is shown in Fig. 9, in this case employing four folders. In addition to the folding stages, a saturator is placed at the output to model the behaviour of an output buffer stage. Table 1 summarizes the component and constant values for the proposed structure. Figure 8(a) shows the result of processing a unity gain sinusoidal input with this structure for  $G = 10$  and zero DC offset. Figure 8(b) illustrates the outcome of processing the same waveform for  $G = 10$  and a DC offset of  $5 \text{ V}$ .

A real-time demo of the proposed topology implemented using Max/MSP and Gen is available at <http://research.spa.aalto.fi/publications/papers/smc17-wavefolder>.

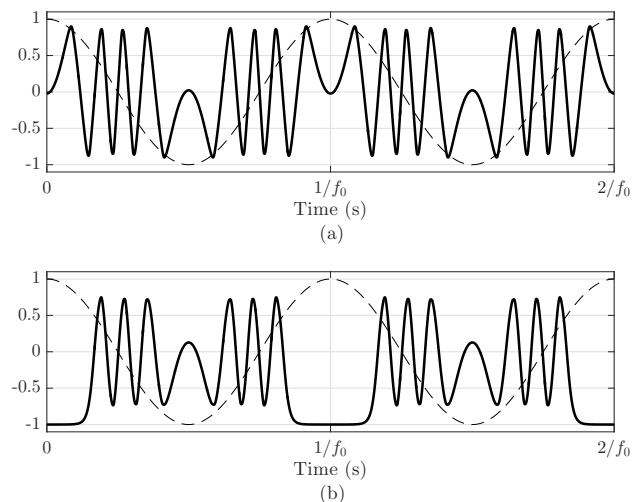


Figure 8. Waveform for a unit gain sine signal processed using the proposed cascaded structure with (a)  $G = 10$  and (b)  $G = 10$  plus a  $5 \text{ V}$  DC offset.

Component	Value	Constant	Value
$R$	$15 \text{ k}\Omega$	$V_T$	$26 \text{ mV}$
$R_L$	$7.5 \text{ k}\Omega$	$I_S$	$10^{-17} \text{ A}$

Table 1. Summary of component and constant values for the proposed cascaded model. Parameter  $F_s = 88.2 \text{ kHz}$ .

## 7. CONCLUSION

In this work we explored the behavior of the Lockhart wavefolder circuit, a West Coast-style nonlinear waveshaper. A VA model of the circuit was then derived using the Lambert-W function. Results obtained were validated against SPICE simulations of the original circuit. To tackle the aliasing caused by the nonlinear nature of wavefolding, the proposed model was extended to incorporate the first-order antiderivative antialiasing method. When combined with oversampling by factor 2, the antialiased wavefolder model is free from perceivable aliasing while still being suitable for real-time implementation.

Furthermore, a proposed synthesis topology consisting of four cascaded wavefolding stages was presented. The recommended structure demonstrates the capabilities of the derived circuit model in a synthesis environment. However, the proposed topology is not unique, as it can be modified according to the needs of the particular application. For instance, the number of stages can be modified. Similarly, the value of the internal load resistance can be increased for added brightness. This effectively showcases the flexibility of VA models.

Future work on the topic of wavefolding will focus on modeling the original Buchla timbre circuit. This kind of work can then extend to the study of other West Coast circuits and synthesis techniques.

## Acknowledgments

The authors would like to thank Prof. Vesa Välimäki for his assistance generating the ANMR curves and for his helpful

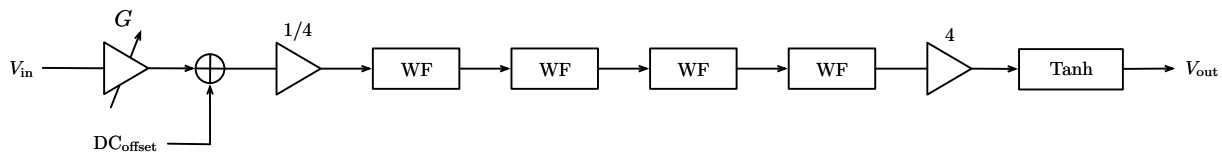


Figure 9. Block diagram for the proposed cascaded waveshaper structure. Input gain and DC offset are used to control the timbre of the output signal.

comments during the final preparation of this work. F. Esqueda is supported by the Aalto ELEC Doctoral School.

## 8. REFERENCES

- [1] R. A. Moog, "A voltage-controlled low-pass high-pass filter for audio signal processing," in *Proc. 7th Conv. Audio Eng. Soc.*, New York, USA, Oct. 1965.
- [2] Buchla Electronic Musical Instruments. The history of Buchla. Accessed March 3, 2017. [Online]. Available: <https://buchla.com/history/>
- [3] J. Parker and S. D'Angelo, "A digital model of the Buchla lowpass-gate," in *Proc. Int. Conf. Digital Audio Effects (DAFx-13)*, Maynooth, Ireland, Sept. 2013.
- [4] K. Stone. Simple wave folder for music synthesizers. Accessed March 3, 2017. [Online]. Available: [http://www.cgs.synth.net/modules/cgs52\\_folder.html](http://www.cgs.synth.net/modules/cgs52_folder.html)
- [5] D. Rossum, "Making digital filters sound "analog"," in *Proc. Intl. Computer Music Conf. (ICMC 1992)*, San Jose, CA, USA, Oct. 1992, pp. 30–34.
- [6] V. Välimäki, S. Bilbao, J. O. Smith, J. S. Abel, J. Pakarinen, and D. Berners, "Introduction to the special issue on virtual analog audio effects and musical instruments," *IEEE Trans. Audio, Speech and Lang. Process.*, vol. 18, no. 4, pp. 713–714, May 2010.
- [7] T. Stilson and J. O. Smith, "Analyzing the Moog VCF with considerations for digital implementation," in *Proc. Int. Computer Music Conf.*, Hong Kong, Aug. 1996.
- [8] A. Huovilainen, "Non-linear digital implementation of the Moog ladder filter," in *Proc. Int. Conf. Digital Audio Effects (DAFx-04)*, Naples, Italy, Oct. 2004, pp. 61–164.
- [9] T. Hélie, "On the use of Volterra series for real-time simulations of weakly nonlinear analog audio devices: application to the Moog ladder filter," in *Proc. Int. Conf. Digital Audio Effects (DAFx-06)*, Montreal, Canada, Sept. 2006, pp. 7–12.
- [10] F. Fontana and M. Civolani, "Modeling of the EMS VCS3 voltage-controlled filter as a nonlinear filter network," *IEEE Trans. Audio, Speech, Language Process.*, vol. 18, no. 4, pp. 760–772, Apr. 2010.
- [11] S. D'Angelo and V. Välimäki, "Generalized Moog ladder filter: Part II – explicit nonlinear model through a novel delay-free loop implementation method," *IEEE/ACM Trans. Audio, Speech, Language Process.*, vol. 22, no. 12, pp. 1873–1883, Dec. 2014.
- [12] A. Huovilainen, "Enhanced digital models for analog modulation effects," in *Proc. Int. Conf. Digital Audio Effects (DAFx-05)*, Madrid, Spain, Sept. 2005, pp. 155–160.
- [13] D. T. Yeh, J. Abel, and J. O. S. III, "Simulation of the diode limiter in guitar distortion circuits by numerical solution of ordinary differential equations," in *Proc. Int. Conf. Digital Audio Effects (DAFx-07)*, Bordeaux, France, Sept. 2007, pp. 197–204.
- [14] J. Pakarinen and D. T. Yeh, "A review of digital techniques for modeling vacuum-tube guitar amplifiers," *Computer Music J.*, vol. 33, no. 2, pp. 85–100, 2009.
- [15] J. Parker, "A simple digital model of the diode-based ring modulator," in *Proc. Int. Conf. Digital Audio Effects (DAFx-11)*, Paris, France, Sept. 2011, pp. 163–166.
- [16] M. Holters and U. Zölzer, "Physical modelling of a wah-wah effect pedal as a case study for application of the nodal dk method to circuits with variable parts," in *Proc. Int. Conf. Digital Audio Effects (DAFx-11)*, Paris, France, Sept. 2011, pp. 31–35.
- [17] R. C. D. de Paiva, J. Pakarinen, V. Välimäki, and M. Tikander, "Real-time audio transformer emulation for virtual tube amplifiers," *EURASIP J. Adv. Signal Process.*, vol. 2011, Feb. 2011.
- [18] D. Yeh, "Automated physical modeling of nonlinear audio circuits for real-time audio effects part II: BJT and vacuum tube examples," *IEEE Trans. Audio, Speech, Language Process.*, vol. 20, no. 4, pp. 1207–126, May 2012.
- [19] F. Eichas, M. Fink, M. Holters, and U. Zölzer, "Physical modeling of the MXR Phase 90 guitar effect pedal," in *Proc. Int. Conf. Digital Audio Effects (DAFx-14)*, Erlangen, Germany, Sept. 2014, pp. 153–158.
- [20] C. Roads, "A tutorial on non-linear distortion or waveshaping synthesis," *Computer Music J.*, vol. 3, no. 2, pp. 29–34, 1979.
- [21] M. L. Brun, "Digital waveshaping synthesis," *J. Audio Eng. Soc.*, vol. 27, no. 4, pp. 250–266, 1979.
- [22] J. Kleimola, "Audio synthesis by bitwise logical modulation," in *Proc. 11th Int. Conf. Digital Audio Effects (DAFx-08)*, Espoo, Finland, Sept. 2008, pp. 60–70.
- [23] J. Kleimola, V. Lazzarini, J. Timoney, and V. Välimäki, "Vector phaseshaping synthesis," in *Proc. 14th Int. Conf. Digital Audio Effects (DAFx-11)*, Paris, France, Sept. 2011, pp. 233–240.
- [24] T. Stilson and J. Smith, "Alias-free digital synthesis of classic analog waveforms," in *Proc. Int. Computer Music Conf.*, Hong Kong, Aug. 1996, pp. 332–335.
- [25] E. Brandt, "Hard sync without aliasing," in *Proc. Int. Computer Music Conf.*, Havana, Cuba, Sept. 2001, pp. 365–368.
- [26] V. Välimäki, "Discrete-time synthesis of the sawtooth waveform with reduced aliasing," *IEEE Signal Process. Lett.*, vol. 12, no. 3, pp. 214–217, Mar. 2005.
- [27] V. Välimäki, J. Nam, J. O. Smith, and J. S. Abel, "Alias-suppressed oscillators based on differentiated polynomial waveforms," *IEEE Trans. Audio Speech Lang. Process.*, vol. 18, no. 4, pp. 786–798, May 2010.
- [28] V. Välimäki, J. Pekonen, and J. Nam, "Perceptually informed synthesis of bandlimited classical waveforms using integrated polynomial interpolation," *J. Acoust. Soc. Am.*, vol. 131, no. 1, pp. 974–986, Jan. 2012.
- [29] E. Brandt, "Higher-order integrated wavetable synthesis," in *Proc. Int. Conf. Digital Audio Effects (DAFx-12)*, York, UK, Sept. 2012, pp. 245–252.
- [30] J. Kleimola and V. Välimäki, "Reducing aliasing from synthetic audio signals using polynomial transition regions," *IEEE Signal Process. Lett.*, vol. 19, no. 2, pp. 67–70, Feb. 2012.
- [31] F. Esqueda, S. Bilbao, and V. Välimäki, "Aliasing reduction in clipped signals," *IEEE Trans. Signal Process.*, vol. 60, no. 20, pp. 5255–5267, Oct. 2016.
- [32] F. Esqueda, V. Välimäki, and S. Bilbao, "Rounding corners with BLAMP," in *Proc. Int. Conf. Digital Audio Effects (DAFx-16)*, Brno, Czech Republic, Sept. 2016, pp. 121–128.
- [33] J. Parker, V. Zavalishin, and E. Le Bivic, "Reducing the aliasing of nonlinear waveshaping using continuous-time convolution," in *Proc. Int. Conf. Digital Audio Effects (DAFx-16)*, Brno, Czech Republic, Sept. 2016, pp. 137–144.
- [34] S. Bilbao, F. Esqueda, J. Parker, and V. Välimäki, "Antiderivative anti-aliasing for memoryless nonlinearities," *IEEE Signal Process. Lett.*, to be published.
- [35] R. Lockhart Jr., "Non-selective frequency tripler uses transistor saturation characteristics," *Electronic Design*, no. 17, Aug. 1973.
- [36] K. J. Werner, V. Nangia, A. Bernardini, J. O. Smith III, and A. Sarti, "An improved and generalized diode clipper model for wave digital filters," in *Proc. 139th Conv. Audio Eng. Soc.*, New York, USA, Oct.–Nov. 2015.
- [37] A. Bernardini, K. J. Werner, A. Sarti, and J. O. S. III, "Modeling nonlinear wave digital elements using the Lambert function," *IEEE Transactions on Circuits and Systems I: Regular Papers*, vol. 63, no. 8, pp. 1231–1242, Aug 2016.
- [38] R. C. D. de Paiva, S. D'Angelo, J. Pakarinen, and V. Välimäki, "Emulation of operational amplifiers and diodes in audio distortion circuits," *IEEE Trans. Circuits Syst. II, Exp. Briefs*, vol. 59, no. 10, pp. 688–692, Oct. 2012.
- [39] D. Veberič. Having fun with Lambert W(x) function. Accessed March 3, 2017. [Online]. Available: <https://arxiv.org/pdf/1003.1628.pdf>
- [40] C. Moler. The Lambert W function. Accessed May 19, 2017. [Online]. Available: <http://blogs.mathworks.com/cleve/2013/09/02/the-lambert-w-function/>
- [41] H.-M. Lehtonen, J. Pekonen, and V. Välimäki, "Audibility of aliasing distortion in sawtooth signals and its implications for oscillator algorithm design," *J. Acoust. Soc. Am.*, vol. 132, no. 4, pp. 2721–2733, Oct. 2012.